Journal of
Mechanics of
Materials and Structures

ANISOTROPY IN HYPOELASTIC SOFT-TISSUE MECHANICS II: SIMPLE EXTENSIONAL EXPERIMENTS

Alan D. Freed

Volume 4, № 6 June 2009

mathematical sciences publishers

JOURNAL OF MECHANICS OF MATERIALS AND STRUCTURES
Vol. 4, No. 6, 2009

ANISOTROPY IN HYPOELASTIC SOFT-TISSUE MECHANICS II: SIMPLE EXTENSIONAL EXPERIMENTS

ALAN D. FREED

Isochoric, hypoelastic, material models are employed to describe the passive response of isotropic and anisotropic soft tissues, using experimental data that have been taken from the literature. The isotropic tissues modeled are elastin and fat, and the anisotropic tissue modeled is tendon. A graphical technique is provided for estimating the material parameters of the anisotropic model, whose values are contrasted with maximum likelihood estimates. All numerical integrations were made with a new 4(3) Runge–Kutta integrator whose quadratures and weights are motivated by finite-element theory.

1. Introduction

Part I of this paper [Freed 2008] departed from longstanding tradition by considering a *hypoelastic* construction for soft tissues, instead of adopting a more conventional *hyperelastic* formulation. In this second part, we extend and apply this theory to a variety of axially loaded, soft-tissue experiments that have been published in the literature.

Hyperelastic materials establish stress via a potential function in strain [Ogden 1984]. Such potentials have their origin in thermodynamics. They produce theories where the value of stress depends only on the current state of strain, and not on the path traversed to reach that state. *Hypoelastic materials* establish stress-rate via a linear function in strain-rate [Truesdell 1955], and have the ability to reach states of stress that are path dependent, in accordance with recent experimental observations [Criscione et al. 2003]. In [Freed 2008], a special class of hypoelastic materials was introduced where stress-rate is given by a potential function in strain-rate. Such potentials must be quadratic in strain-rate so as to remain compatible with Truesdell's general definition of a hypoelastic material. The definition for hypoelastic materials given here is similar in mathematical structure to the classic construct of hyperelastic materials, it is just that the independent and dependent variables are now in rate form.

What motivated this researcher to consider hypoelasticity over hyperelasticity for describing the passive response of soft tissues is the fact that ever since Fung's pioneering work [1967], we have known that the stress/strain response of soft tissues is, to a good approximation, exponential. For the ensuing forty years, tissue mechanicians have proposed numerous ways to incorporate this exponential property into their hyperelastic frameworks. All of these seem rather ad hoc to me; whereas, hypoelasticity, being a rate theory, has the exponential character of its solution built in, so to speak (the characteristic solution of a first-order differential equation is an exponential). Consequently, the hypoelastic viewpoint should allow for a more satisfying theory to be constructed. This paper is but a step in that direction.

MSC2000: 74B20, 74L15.

Keywords: anisotropy, calcaneal fat pad, elastin, fascia lata, finite deformation, hypoelasticity, log likelihood, parameter estimation, Runge–Kutta integrator.

An application of hypoelastic models requires solving systems of ordinary differential equations (ODEs) satisfying initial conditions (ICs). Analytic solutions are available for only the simplest boundary conditions (BCs). Most BCs will require numerical solutions, with the more complex problems requiring finite-element (FE) analysis. Such BCs may describe an experiment whose purpose is to establish the parameters of a model, or they may specify a more challenging problem, like the interaction between neighboring tissues and a bioprosthetic implant. The method of solution that one chooses will be BC dependent. In this paper, the sole purpose for solving BCs is to acquire parameter estimates for models. For this purpose, the optimization strategy and the Runge–Kutta integrator of Appendices A and B, respectively, have been employed.

Hypoelastic models present a new set of challenges over traditional hyperelastic models in their implementation into FE codes. The consistent tangent matrix for a material model is typically required by codes designed to analyze solid bodies [Holzapfel 2000]. Their construction is more amenable to the stress/strain relations of hyperelastic materials than it is to the stress-rate/strain-rate relations of hypoelastic materials. In the case of the latter, an efficient integration algorithm, local at the Gauss point, must also accompany the model. It is often the efficiency of such an integrator that determines whether or not a particular rate-model is viable. Fluids codes, being rate codes, and hypoelasticity, being a rate theory, suggest a different avenue. Computational fluid dynamics (CFD) codes may be the better choice for implementing a hypoelastic material model. This is speculation at this time, and will be the topic of future research.

This paper begins with a synopsis of the isochoric, hypoelastic, constitutive model for isotropic soft tissues derived in [Freed 2008]. Solutions for this material model are provided for the BCs of uniaxial, equibiaxial, laterally constrained, and pure-shear extensions. There are no off-diagonal components in the deformation gradients that describe these experiments. It is shown that for isochoric hypoelastic materials, the BC for laterally-constrained extension does not reproduce the stress state caused by the BC for pure shear, like occurs with isochoric hyperelastic models.

The next section extends our isotropic theory to one that is suitable for anisotropic materials through the introduction of an anisotropy tensor, which is a material tensor that was given a geometric interpretation in [Freed 2008]. Invariant theory is called upon to construct a potential function, through which an anisotropic, isochoric, hypoelastic, constitutive equation is derived. Physical arguments are used to reduce the numbers-of and combinations-between pertinent invariants. A tensor function is introduced to address the physical observations that: collagen fibrils do not support compressive or hydrostatic states of stress, and their response becomes linear after their crimp has stretched straight. The resulting constitutive equation has been solved for the BCs of: uniaxial and laterally-constrained extensions stretched in the fiber direction, uniaxial extensions stretched normal to the fiber direction, and equibiaxial extensions where the fibers align with one of the two loading axes. The anisotropy considered here describes a single-fiber family with a fiber dispersion that projects onto the transverse plane in the reference state as a circular disk.

This theoretical discussion is followed by a results section where numerical solutions are presented for these two, hypoelastic, material models. Elastin and the calcaneal fat pad are modeled as isotropic hypoelastic materials, while tendon (fascia lata) is modeled as an anisotropic hypoelastic material. The paper concludes with a discussion of the hypoelastic models presented, along with some of the results obtained.

A maximum likelihood algorithm is outlined in the Appendix A, with an emphasis toward acquiring parameter estimates for models described by ODEs satisfying an IC, like hypoelastic material models. Also presented in Appendix B is a new, embedded, Runge–Kutta method that has proved to be both accurate and reliable for solving nonstiff systems of nonlinear ODEs.

Preliminaries. Scalars are typeset in italics, for example, y. Vectors are typeset in lower-case bold italics, for example, $\boldsymbol{y} = y_i \boldsymbol{e}_i$. Tensors are typeset in upper-case bold italics, for example, $\boldsymbol{Y} = Y_{ij} \boldsymbol{e}_i \otimes \boldsymbol{e}_j$, where $\otimes$ is the tensor product. Components y_i and Y_{ij} are also typeset in italics, and are quantified in a rectangular Cartesian basis $\{\boldsymbol{e}_1, \boldsymbol{e}_2, \boldsymbol{e}_3\}$. Exceptions to this notation are minimal, but they do arise, typically for historical reasons.

Polar tensors, like $\bar{\boldsymbol{Y}}$, relate to their Eulerian counterparts, in this case $\boldsymbol{Y}$, via the mapping $\bar{\boldsymbol{Y}} = \boldsymbol{R}^T \boldsymbol{Y} \boldsymbol{R}$, where $\boldsymbol{R}$ is the rotation tensor from a polar decomposition of the deformation gradient tensor $\boldsymbol{F}$. The material derivative of a polar field $\dot{\bar{\boldsymbol{Y}}}$ maps into the Eulerian frame as $\dot{\bar{\boldsymbol{Y}}} = \boldsymbol{R}^T \hat{\boldsymbol{Y}} \boldsymbol{R}$, where $\hat{\boldsymbol{Y}}$ denotes the polar rate of $\boldsymbol{Y}$ defined by $\hat{\boldsymbol{Y}} = \dot{\boldsymbol{Y}} - \boldsymbol{\Omega Y} + \boldsymbol{Y \Omega}$ [Dienes 1987], which is the objective rate of [Green and Naghdi 1965], with tensor $\boldsymbol{\Omega} = \dot{\boldsymbol{R}} \boldsymbol{R}^T$ defining spin, or the rate of rigid-body rotation (compare [Dienes 1979]).

2. Isotropic hypoelastic model

Most biological tissues are anisotropic, but there are a few tissues that are essentially isotropic, of which elastin and fat are examples, and are modeled in Section 4.1.

In [Freed 2008] we derived the constitutive equation for an isotropic hypoelastic tissue from the potential equation

$$\dot{\bar{\boldsymbol{T}}} = \frac{\partial \Psi(\bar{\boldsymbol{T}}, \dot{\bar{\boldsymbol{E}}})}{\partial \dot{\bar{\boldsymbol{E}}}}, \tag{1}$$

where tensor $\boldsymbol{T}$ is the Kirchhoff stress, and tensor $\hat{\boldsymbol{E}}$ is the polar rate of strain (it is synonymous with the stretching tensor $\boldsymbol{D} = \operatorname{sym} \boldsymbol{L}$, where $\boldsymbol{L} = \dot{\boldsymbol{F}} \boldsymbol{F}^{-1}$ is the velocity gradient tensor). Polar equivalents to these Eulerian fields, which are used above, are gotten through standard mappings; in particular, $\bar{\boldsymbol{T}} = \boldsymbol{R}^T \boldsymbol{T} \boldsymbol{R}$, $\dot{\bar{\boldsymbol{T}}} = \boldsymbol{R}^T \hat{\boldsymbol{T}} \boldsymbol{R}$ and $\dot{\bar{\boldsymbol{E}}} = \boldsymbol{R}^T \hat{\boldsymbol{E}} \boldsymbol{R} \equiv \boldsymbol{R}^T \boldsymbol{D} \boldsymbol{R}$.

Because the two arguments $\bar{\boldsymbol{T}}$ and $\dot{\bar{\boldsymbol{E}}}$ of the scalar potential Ψ are symmetric tensor fields, they can be replaced with ten scalar invariants [Rivlin and Smith 1969]. This number can be reduced by imposing Truesdell's [1955] definition for a hypoelastic solid, which requires each term in Ψ to be quadratic in strain-rate; by imposing Fung's law [1967], which restricts each term in Ψ to be at most linear in stress; and by imposing an isochoric constraint, $\operatorname{tr} \dot{\bar{\boldsymbol{E}}} = 0$. From these restrictions, one arrives at the most general form that potential Ψ can have; it being [Freed 2008]

$$\Psi = \mu \operatorname{tr}(\dot{\bar{\boldsymbol{E}}} \dot{\bar{\boldsymbol{E}}}) + \alpha \tfrac{1}{3} \operatorname{tr}(\bar{\boldsymbol{T}}) \operatorname{tr}(\dot{\bar{\boldsymbol{E}}} \dot{\bar{\boldsymbol{E}}}) + \beta \operatorname{tr}(\bar{\boldsymbol{T}} \dot{\bar{\boldsymbol{E}}} \dot{\bar{\boldsymbol{E}}}) - \dot{\wp} (\operatorname{tr} \dot{\bar{\boldsymbol{E}}} - 0). \tag{2}$$

where scalar $\dot{\wp}$ is a Lagrange multiplier forcing an isochoric (constant volume) response, and α, β and μ are material constants: μ has units of stress, it being the small-strain shear modulus, while parameters α and β are both dimensionless, governing the rate of exponential growth in stress with increasing strain, with α accounting for the response due to hydrostatic pressure. Substituting this potential into (1) gives

the constitutive equation for an isotropic, isochoric, hypoelastic tissue, which is

$$\dot{\bar{\boldsymbol{T}}} + \dot{\wp}\bar{\boldsymbol{I}} = 2(\mu - \alpha p)\dot{\bar{\boldsymbol{E}}} + \beta(\bar{\boldsymbol{T}}\dot{\bar{\boldsymbol{E}}} + \dot{\bar{\boldsymbol{E}}}\bar{\boldsymbol{T}}), \tag{3}$$

where scalar $p = -\frac{1}{3}\operatorname{tr}\boldsymbol{T}$ is the hydrostatic pressure, which is distinct from the Lagrange multiplier $\wp$. This is an advantage over isochoric hyperelastic models, which cannot distinguish p from $\wp$ in their constructs. ODE (3) is subject to an IC of $\bar{\boldsymbol{T}}(0) = \bar{\boldsymbol{T}}_0$.

Classic boundary value problems. Three experiments are commonly employed to estimate the material parameters of isotropic, isochoric, hyperelastic solids used to model rubbery materials; they are: uniaxial extension, equibiaxial extension, and pure shear [Treloar 1975], of which any two are sufficient for a complete characterization. Unlike hyperelastic models, hypoelastic models can respond to the presence of hydrostatic pressure. Consequently, as shown below, stress states from the BC of a laterally-constrained extension does not reproduce the stress state from the BC of pure shear in hypoelastic materials, as they do in hyperelastic materials.

Uniaxial and equibiaxial extensions. For the isotropic, isochoric, hypoelastic material described by (3), the BC for uniaxial extension is quantified by the ODE[1]

$$\frac{\mathrm{d}\tau}{\mathrm{d}\lambda} = \frac{3\mu + (\alpha + 2\beta)\tau}{\lambda}, \tag{4}$$

while the BC for equibiaxial extension is governed by

$$\frac{\mathrm{d}\tau}{\mathrm{d}\lambda} = 2\frac{3\mu + (2\alpha + \beta)\tau}{\lambda}, \tag{5}$$

wherein τ is the Kirchhoff (true or Cauchy) stress, and λ is the applied stretch, with a typical IC being $\tau(1) = 0$. Equations (4) and (5), satisfying this IC, have an analytic solution of the form $\tau = \frac{a}{b}\left(\mathrm{e}^{b\ln\lambda} - 1\right)$, where $a = 3\mu$ and $b = \alpha + 2\beta$ for uniaxial extension, and $a = 6\mu$ and $b = 4\alpha + 2\beta$ for equibiaxial extension. This solution is expressed in terms of the natural (true or Hencky) strain.

In the small-strain limit, uniaxial extension has a modulus of 3μ, while equibiaxial extension has a modulus of 6μ, which agree with predictions from the classic theory for rubber elasticity [Treloar 1975]. Whenever $\alpha = \beta$, the same ratio of 3:6 exists between their tangent moduli throughout the nonlinear region. However, whenever $\alpha \neq \beta$, hypoelasticity is capable of predicting different, nonlinear, stress/strain responses for these two experiments. This is because, unlike isochoric hyperelastic models, the affect of hydrostatic pressure is handled by isochoric hypoelastic models. This is apparent in (4) and (5), where equibiaxial extension has twice the pressure content of uniaxial extension, and four times the effect.

Either experiment, by itself, is incapable of delineating α from β. As a minimum, two excursions into stretch/stress space, whose deformations extend well into the nonlinear region, and that possess different hydrostatic states, like uniaxial and equibiaxial extensions, are needed in order to be able to acquire a complete characterization of all three parameters in this simple material model.

[1] Equation (4) is nearly, but not exactly, equal to Fung's law [1967] $\mathrm{d}\sigma/\mathrm{d}\lambda = E + \gamma\sigma$, where $\sigma = \tau/\lambda$ is the engineering stress and E and γ are material constants. In his paper, Fung spent a lot of effort addressing what is, effectively, the correct initial condition to impose, from the experimentalist's point of view, and how it manifests itself in the integrated solution of his law.

An application of the chain rule allowed stretch to replace time as the independent variable in (4) and (5); hence, hypoelasticity can be used to model quasistatic experiments.

Pure shear. A state of pure shear is achieved by extending a block of material in one direction by some amount λ, while simultaneously compressing it in a lateral direction by λ^{-1}, with the third orthogonal direction remaining fixed in length and free from traction. This is a difficult BC to achieve experimentally. For the isotropic, isochoric, hypoelastic material of (3), the pure shear BC is described by the ODEs

$$\frac{\mathrm{d}\tau_i}{\mathrm{d}\lambda_i} = \pm 2\frac{\mu + \beta\tau_i}{\lambda_i}, \quad i = 1, 2, \tag{6}$$

which are independent of pressure — the hallmark of pure shear — as parameter α is not present. Here $i = 1$ associates with the plus sign, and that direction where stretch is λ; while $i = 2$ associates with the minus sign, and that direction where stretch is λ^{-1}. Mohr's circle is centered at the origin, with its two circumscribed circles having equal diameters, and as such, this stress state is free from hydrostatic pressure.

Laterally constrained axial extensions. Pure-shear experiments done on elastomers typically apply an axial extension to a short but very wide sheet of material, relying on the lateral constraint of the grips to effectively keep the lateral principal stretch fixed at one (compare [Treloar 1975]). An indirect consequence of the isochoric constraint, when applied to hyperelastic solids, is that any translation of Mohr's circle is nonphysical, because these models cannot distinguish between hydrostatic pressure and their isochoric Lagrange multiplier. Consequently, because the two circumscribed Mohr's circles have the same diameter for both the laterally constrained and pure shear BCs, these BCs produce equivalent states of stress when imposed on isochoric hyperelastic materials.

In contrast, the BC of laterally constrained axial extension does not produce a stress state that is akin to pure shear when applied to an isochoric hypoelastic solid, because hypoelastic materials can support hydrostatic pressures, so translations of Mohr's circle remain physical in hypoelastic models. For the isotropic, isochoric, hypoelastic tissues obeying (3), the stretching of a short wide sheet is described by the ODEs

$$\frac{\mathrm{d}\tau_1}{\mathrm{d}\lambda} = 2\frac{2\mu + \frac{2}{3}\alpha(\tau_1 + \tau_2) + \beta\tau_1}{\lambda} \quad \text{and} \quad \frac{\mathrm{d}\tau_2}{\mathrm{d}\lambda} = \frac{2\mu + \frac{2}{3}\alpha(\tau_1 + \tau_2)}{\lambda}, \tag{7}$$

where τ_1 is the stress in the applied stretch direction, τ_2 is the stress in the lateral direction along the grips, and λ is the applied stretch. These formulæ are distinct from those that govern pure shear in (6).

3. Anisotropic hypoelastic model

The potential equation (1) describing an isotropic hypoelastic tissue can be extended straightaway for anisotropic tissues by introducing a structural tensor $\bar{\boldsymbol{A}}$ [Freed 2008; Freed et al. 2005; Gasser et al. 2006] into its argument list so that

$$\mathring{\bar{\boldsymbol{T}}} = \frac{\partial\Psi(\bar{\boldsymbol{A}}, \bar{\boldsymbol{T}}, \mathring{\bar{\boldsymbol{E}}})}{\partial\mathring{\bar{\boldsymbol{E}}}}, \tag{8}$$

where tensor $\bar{\boldsymbol{A}}$ is a physical constant in the sense of [Oldroyd 1950]. This is the anisotropy tensor, and it is normalized so that $\|\bar{\boldsymbol{A}}\|_2 = 1$ for geometric reasons [Freed 2008].

The three symmetric tensors that are the arguments of Ψ can be replaced with twenty-eight scalar invariants [Rivlin and Smith 1969]. By applying the same reasoning used to reduce the set of invariants that lead to (2); by imposing our geometric restriction that the anisotropy tensor $\bar{\boldsymbol{A}}$ attenuates deformations, not loads, and is a material constant [Freed 2008]; by introducing a mechanism to account for the fact that collagen fibrils are one-dimensional structures in soft tissues that do not support compressive or hydrostatic loads (these are handled by the surrounding matrix); and finally, by introducing another mechanism to provide for a smooth transition between the nonlinear and linear regions in a typical stress-stretch curve for soft tissue, which is caused by the stretching of crimped collagen; one is eventually lead to the potential

$$\Psi = \mu\,\mathrm{tr}(\dot{\bar{\boldsymbol{E}}}\,\bar{\boldsymbol{A}}\,\dot{\bar{\boldsymbol{E}}}) + \alpha\tfrac{1}{3}\,\mathrm{tr}(\bar{\boldsymbol{T}})\,\mathrm{tr}(\dot{\bar{\boldsymbol{E}}}\,\bar{\boldsymbol{A}}\,\dot{\bar{\boldsymbol{E}}}) + \beta\,\mathrm{tr}(\overline{\mathcal{T}}\,\dot{\bar{\boldsymbol{E}}}\,\bar{\boldsymbol{A}}\,\dot{\bar{\boldsymbol{E}}}) - \dot{\wp}(\mathrm{tr}\,\dot{\bar{\boldsymbol{E}}} - 0), \tag{9}$$

which produces the following constitutive equation for an anisotropic, isochoric, hypoelastic tissue[2]

$$\dot{\bar{\boldsymbol{T}}} + \dot{\wp}\,\bar{\boldsymbol{I}} = (\mu - \alpha p)\left(\dot{\bar{\boldsymbol{E}}}\,\bar{\boldsymbol{A}} + \bar{\boldsymbol{A}}\,\dot{\bar{\boldsymbol{E}}}\right) + \beta\left(\overline{\mathcal{T}}\,\dot{\bar{\boldsymbol{E}}}\,\bar{\boldsymbol{A}} + \bar{\boldsymbol{A}}\,\dot{\bar{\boldsymbol{E}}}\,\overline{\mathcal{T}}\right), \tag{10}$$

where, in addition to the material parameters μ, α and β of the isotropic model, one has to also quantify the five independent components of $\bar{\boldsymbol{A}}$ that describe the tissue's anisotropy, recalling that $\|\bar{\boldsymbol{A}}\|_2 = 1$, and to establish a mathematical structure for the symmetric tensor function $\overline{\mathcal{T}}$.

The polar stress $\bar{\boldsymbol{T}}$ has been replaced by a tensor valued function $\overline{\mathcal{T}} = \boldsymbol{R}^T\mathcal{T}\,\boldsymbol{R}$ in the β term of (9) and (10). This function is introduced into the phenomenological relationship to address the physical restrictions that collagen fibrils are tension-only structures with helical geometries in their unloaded state, and that these helices stretch straight under deformation [Freed and Doehring 2005]. The tensor function considered is

$$\mathcal{T}(\boldsymbol{T}) = \boldsymbol{Q}^T\widetilde{\mathcal{T}}\,\boldsymbol{Q} \quad \text{wherein} \quad \widetilde{\mathcal{T}} = \begin{bmatrix} f(\tau_1) & 0 & 0 \\ 0 & f(\tau_2) & 0 \\ 0 & 0 & f(\tau_3) \end{bmatrix} \quad \text{and} \quad Q_{ij} = \tilde{\boldsymbol{e}}_i \cdot \boldsymbol{e}_j, \tag{11}$$

so that $\overline{\mathcal{T}} = \boldsymbol{R}^T\,\boldsymbol{Q}^T\widetilde{\mathcal{T}}\,\boldsymbol{Q}\boldsymbol{R}$, where the eigenvalues τ_i and eigenvectors $\tilde{\boldsymbol{e}}_i$ arise from a spectral representation of the Kirchhoff stress $\boldsymbol{T}$, and are normalized so that $\boldsymbol{I} = \tilde{\boldsymbol{e}}_i \otimes \tilde{\boldsymbol{e}}_j$ $(i, j = 1, 2, 3)$. Orthogonal tensor $\boldsymbol{Q}$ is a mapping between the spectral $\{\tilde{\boldsymbol{e}}_1, \tilde{\boldsymbol{e}}_2, \tilde{\boldsymbol{e}}_3\}$ and spatial $\{\boldsymbol{e}_1, \boldsymbol{e}_2, \boldsymbol{e}_3\}$ base vectors, while orthogonal tensor $\boldsymbol{R}$ is a mapping between the polar $\{\bar{\boldsymbol{e}}_1, \bar{\boldsymbol{e}}_2, \bar{\boldsymbol{e}}_3\}$ and spatial $\{\boldsymbol{e}_1, \boldsymbol{e}_2, \boldsymbol{e}_3\}$ base vectors. The dimensionless function f is taken to be the ramped step

$$f(\tau) = \begin{cases} 1 & \text{if} \quad \tau > \tau^\star, \\ \tau/\tau^\star & \text{if} \quad 0 \le \tau \le \tau^\star, \\ 0 & \text{if} \quad \tau < 0, \end{cases} \tag{12}$$

with $\tau^\star$ establishing a threshold stress beyond which collagen crimp is stretched straight. This choice of stress function, in conjunction with our hypoelastic formulation, will enable stress/stretch curves typical of many tissues to be modeled; specifically, those where there is a shallow sloped toe region followed

[2]Proposition 1 in [Freed 2008] is not employed here. It was found during the process of writing this document that the decoupling of strain rate into separate fiber and matrix constituents, defined according to that hypothesis, lead to constitutive formulæ that could not accommodate the large difference in shear moduli present in the data for human fascia lata from [1994] that are modeled here.

by a heel that transitions into a linear true stress/strain response that, in a stress/stretch plot, will have slight curvature. If the tissue of interest does not have this type of stress/strain behavior, then a different function for $\mathcal{T}$ will be needed.

In accordance with the above definition for $\mathcal{T}$, the material constants in the anisotropic constitutive equation (10) have slightly different physical interpretations from those of the isotropic constitutive equation (3); specifically, μ is the tissue modulus when collagen is behaving like a helical spring, while β is the tissue modulus at those stresses $\tau_i > \tau^\star$ where collagen has stretched straight. These ideas have been developed in [Freed and Doehring 2005] and works cited therein, to model the response of collagen fibrils. The parameters μ, β and $\tau^\star$ all have units of stress, while α remains dimensionless and retains its prior physical interpretation.

Uniform extensions. There is a versatility in the present theory in that any, admissible, anisotropy tensor $\bar{\boldsymbol{A}}$ can be incorporated into the above constitutive framework without altering its construction. Various $\bar{\boldsymbol{A}}$ tensors belonging to the class of single-fiber families with elliptic projections onto the transverse plane of the reference configuration can be found in [Freed 2008].

It has been demonstrated, for example, that fiber branching is physiologically necessary to stabilize the left ventricle wall, thereby ensuring proper heart function [Niederer et al. 2004]. In their study, splay was described as a single-fiber family with an elliptic projection onto the transverse plane.

The formulæ that follow are applications of the anisotropic, hypoelastic, isochoric tissue given by (10) to four separate BCs that are extensional loadings. In each case, anisotropy is considered to belong to a single-fiber family where the geometric arrangement of fiber orientation at a mass point is encased by a cone in the polar frame, and whose matrix representation is

$$\bar{\boldsymbol{A}} = \begin{bmatrix} 1 & 0 & 0 \\ 0 & \delta & 0 \\ 0 & 0 & \delta \end{bmatrix}, \tag{13}$$

where the angle of mean fiber orientation has been chosen to align with the 1-direction. The scalar δ, which satisfies $0 \le \delta \le 1$, has a statistical origin [Freed et al. 2005; Gasser et al. 2006]. It is the dispersion parameter quantifying the extent of fiber splay.

Other tissues, like arteries [Holzapfel et al. 2002], will require orthotropic anisotropy tensors that belong to material classes with two or more fiber families. Such tissues are not addressed in this paper.

Extensions in the mean fiber direction. Here a specimen is loaded in the fiber- or 1-direction by a stretch of λ. Given that the tissue has an anisotropy described by (13), the constitutive equation (10) produces the matrix equation

$$\begin{bmatrix} \dot{\tau} & 0 & 0 \\ 0 & 0 & 0 \\ 0 & 0 & 0 \end{bmatrix} + \begin{bmatrix} \dot{\wp} & 0 & 0 \\ 0 & \dot{\wp} & 0 \\ 0 & 0 & \dot{\wp} \end{bmatrix} = 2\left(\mu + \alpha\frac{\tau}{3}\right) \begin{bmatrix} \dot{\lambda}/\lambda & 0 & 0 \\ 0 & -\delta\dot{\lambda}/2\lambda & 0 \\ 0 & 0 & -\delta\dot{\lambda}/2\lambda \end{bmatrix} + 2\beta \begin{bmatrix} f(\tau)\dot{\lambda}/\lambda & 0 & 0 \\ 0 & 0 & 0 \\ 0 & 0 & 0 \end{bmatrix}. \tag{14}$$

Substituting the equation for the Lagrange multiplier $\dot{\wp}$ (the equations associated with the second or third rows) into the equation for the Kirchhoff stress, and multiplying through by $\mathrm{d}t/\mathrm{d}\lambda$, one arrives at the governing ODE for this BC, which is

$$\frac{\mathrm{d}\tau}{\mathrm{d}\lambda} = \frac{2+\delta}{3}\frac{3\mu+\alpha\tau}{\lambda} + 2\beta\frac{f(\tau)}{\lambda}, \tag{15}$$

a typical IC being $\tau(1) = 0$.

Extensions normal to the mean fiber direction. Here a specimen is loaded normal to the fiber alignment, or in the 2-direction, by a stretch of λ. Given that the tissue has an anisotropy described by (13), the constitutive equation (10) produces the matrix equation

$$\begin{bmatrix} 0 & 0 & 0 \\ 0 & \dot{\tau} & 0 \\ 0 & 0 & 0 \end{bmatrix} + \begin{bmatrix} \dot{\wp} & 0 & 0 \\ 0 & \dot{\wp} & 0 \\ 0 & 0 & \dot{\wp} \end{bmatrix} = 2\left(\mu + \alpha\frac{\tau}{3}\right)\begin{bmatrix} -\nu\dot{\lambda}/\lambda & 0 & 0 \\ 0 & \delta\dot{\lambda}/\lambda & 0 \\ 0 & 0 & \delta(\nu-1)\dot{\lambda}/\lambda \end{bmatrix} + 2\beta\begin{bmatrix} 0 & 0 & 0 \\ 0 & \delta f(\tau)\dot{\lambda}/\lambda & 0 \\ 0 & 0 & 0 \end{bmatrix}, \tag{16}$$

where ν accommodates variations in the Poisson contraction between the directions that are parallel-with and transverse-to the mean fiber direction. Equating the two equations for the Lagrange multiplier $\dot{\wp}$ leads to the relationship $\delta = \nu/(1-\nu)$, which inverts as $\nu = \delta/(1+\delta)$; consequently, because $0 \le \delta \le 1$, it follows that $0 \le \nu \le 1/2$. The ODE governing Kirchhoff stress for this BC is

$$\frac{\mathrm{d}\tau}{\mathrm{d}\lambda} = \frac{2\delta(2+\delta)}{3(1+\delta)}\frac{3\mu+\alpha\tau}{\lambda} + 2\delta\beta\frac{f(\tau)}{\lambda}, \tag{17}$$

which also has a typical IC of $\tau(1) = 0$.

Laterally constrained extensions in the mean fiber direction. This is basically the same experiment as axial extension, except that Poisson contraction in the 2-direction is not allowed. Given that the tissue has an anisotropy described by (13), the constitutive equation (10) produces the matrix equation

$$\begin{bmatrix} \dot{\tau}_1 & 0 & 0 \\ 0 & \dot{\tau}_2 & 0 \\ 0 & 0 & 0 \end{bmatrix} + \begin{bmatrix} \dot{\wp} & 0 & 0 \\ 0 & \dot{\wp} & 0 \\ 0 & 0 & \dot{\wp} \end{bmatrix} = 2\left(\mu + \alpha\frac{\tau_1+\tau_2}{3}\right)\begin{bmatrix} \dot{\lambda}/\lambda & 0 & 0 \\ 0 & 0 & 0 \\ 0 & 0 & -\delta\dot{\lambda}/\lambda \end{bmatrix} + 2\beta\begin{bmatrix} f(\tau_1)\dot{\lambda}/\lambda & 0 & 0 \\ 0 & 0 & 0 \\ 0 & 0 & 0 \end{bmatrix}, \tag{18}$$

where τ_1 is the Kirchhoff stress in the direction of applied traction, and τ_2 is the Kirchhoff stress in the lateral direction of constraint, which is usually not measured in these experiments. Substituting the equation for the Lagrange multiplier $\dot{\wp}$ into the two equations for the principal Kirchhoff stresses results in two ODEs that describe this BC, they being

$$\frac{\mathrm{d}\tau_1}{\mathrm{d}\lambda} = \frac{2(1+\delta)}{3}\frac{3\mu+\alpha(\tau_1+\tau_2)}{\lambda} + 2\beta\frac{f(\tau_1)}{\lambda} \quad \text{and} \quad \frac{\mathrm{d}\tau_2}{\mathrm{d}\lambda} = \frac{2\delta}{3}\frac{3\mu+\alpha(\tau_1+\tau_2)}{\lambda}, \tag{19}$$

which have typical ICs of $\tau_1(1) = \tau_2(1) = 0$. The presence of parameter α indicates that this deformation contains a hydrostatic pressure, and is therefore not a pure-shear deformation.

Equibiaxial extensions. For isotropic materials, it makes no difference whether the traction or the stretches are maintained equal in an equibiaxial experiment; it does, however, make a difference for anisotropic materials. Here we consider the case where the two orthogonal stretches are maintained equal, with fiber alignment being in the 1-direction. Given that the tissue has an anisotropy that is described by (13), the constitutive equation (10) produces the matrix equation

$$\begin{bmatrix} \dot{\tau}_1+\dot{\wp} & 0 & 0 \\ 0 & \dot{\tau}_2+\dot{\wp} & 0 \\ 0 & 0 & \dot{\wp} \end{bmatrix} = 2\left(\mu+\alpha\frac{\tau_1+\tau_2}{3}\right)\begin{bmatrix} \dot{\lambda}/\lambda & 0 & 0 \\ 0 & \delta\dot{\lambda}/\lambda & 0 \\ 0 & 0 & -2\delta\dot{\lambda}/\lambda \end{bmatrix} + 2\beta\begin{bmatrix} f(\tau_1)\dot{\lambda}/\lambda & 0 & 0 \\ 0 & f(\tau_2)\delta\dot{\lambda}/\lambda & 0 \\ 0 & 0 & 0 \end{bmatrix}. \tag{20}$$

Substituting the equation for the Lagrange multiplier $\dot{\wp}$ into the two equations for the principal Kirchhoff stresses results in the governing ODEs for this BC, they being

$$\frac{\mathrm{d}\tau_1}{\mathrm{d}\lambda} = \frac{2(1+\delta)}{3}\frac{3\mu+\alpha(\tau_1+\tau_2)}{\lambda} + 2\beta\frac{f(\tau_1)}{\lambda} \quad \text{and} \quad \frac{\mathrm{d}\tau_2}{\mathrm{d}\lambda} = \delta\frac{3\mu+\alpha(\tau_1+\tau_2)}{\lambda} + 2\delta\beta\frac{f(\tau_2)}{\lambda}, \tag{21}$$

which have typical ICs of $\tau_1(1) = \tau_2(1) = 0$. There is only a slight difference in the formulæ for $\mathrm{d}\tau_2/\mathrm{d}\lambda$ between (19) and (21), while their formulæ for $\mathrm{d}\tau_1/\mathrm{d}\lambda$ are identical.

4. Results

Our hypoelastic theory is now applied to a few examples where experimental data have been taken from the literature. Purified elastin and the calcaneal fat pad are modeled as isotropic materials, while the fascia lata tendon is modeled as an anisotropic material. The numerical optimization and integration algorithms used to obtain estimates for the material parameters are outlined in two appendices.

4.1. ***Elastin and fat.*** The author is not aware of a single, published, experimental, data set for an isotropic soft tissue that is sufficient to unambiguously quantify all three material parameters associated with (3). In the examples that follow, either α or β is assigned to be zero, a priori; specifically, it is supposed that $\alpha = 0$ for fibrous tissues, and that $\beta = 0$ for nonfibrous tissues. This is conjecture until such time when experimental data become available to test its validity.

Aaron and Gosline [1981] performed uniaxial quasistatic experiments on purified elastin fibers (5–8 μm in diameter) extracted from the bovine ligamentum nuchae. They were tested in distilled water at 24°C. Because fibers are one-dimensional structures, it is expected that they cannot support hydrostatic states, and as such, we set $\alpha = 0$ in this case. Figure 1 shows a fitting of (4) to the experimental data of [Aaron and Gosline 1981], and yields material constants with 90% confidence intervals of $\mu = 0.210 \pm 0.048$ MPa and $\beta = 1.53 \pm 0.19$, with a coefficient of determination of $R^2 = 0.976$.

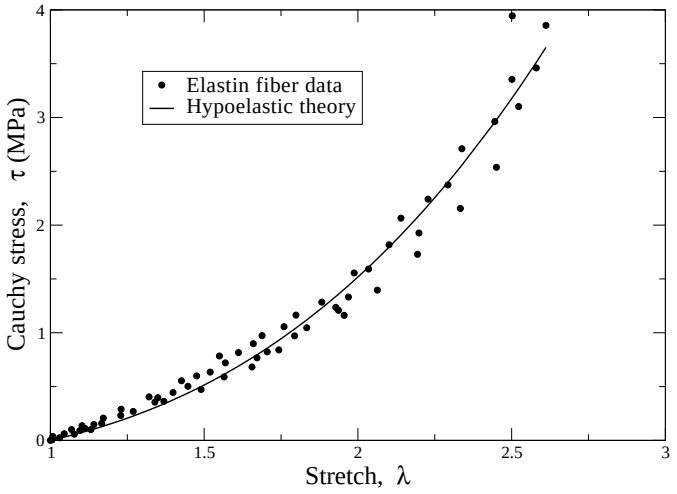

Figure 1. Hypoelastic theory contrasted with experimental data for elastin fibers (5–8 μm in diameter) tested in simple extension, where $\mu = 0.21$ MPa and $\beta = 1.5$, taking $\alpha = 0$. The data are from [Aaron and Gosline 1981, Figure 2a].

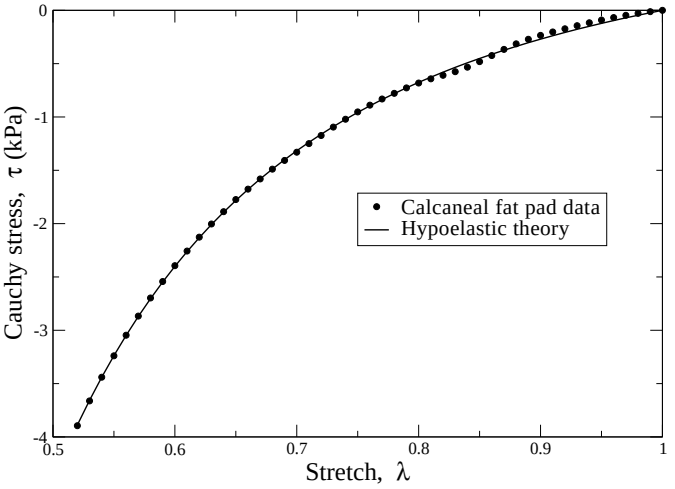

Figure 2. Hypoelastic theory contrasted with experimental data for the human, calcaneal, fat pad ($N = 10$) tested in simple compression, where $\mu = 0.74$ kPa and $\alpha = -2.64$, taking $\beta = 0$. The data are from [Miller-Young et al. 2002, Figure 3].

Miller-Young et al. [2002] performed compression experiments on the human, calcaneal, fat pad excised from the feet of cadavers. They were tested in air at ambient temperature. Because the calcaneal fat pad operates predominantly in a hydrostatic environment, one would expect parameter α to dominate over β, and as such, we have set $\beta = 0$ in this case. A fitting of (4) to the mean curve constructed from averaging ten quasistatic experiments, each from an individual specimen, yields material constants with 90% confidence intervals of $\mu = 0.741 \pm 0.016$ kPa and $\alpha = -2.638 \pm 0.063$, with a coefficient of determination of $R^2 = 0.999$. (See Figure 2.) The averaging of data over ten experiments contributed to the high R^2 value obtained here. The reported standard deviation for experimental variability around the mean stress for these ten experiments was about $\pm 10\%$ at the point of maximum compression [Miller-Young et al. 2002].

4.2. ***Algorithm for graphical estimation of model parameters.*** Hypoelastic constitutive equations are rate models. This suggests that estimates for its material constants could be tangents to specific response curves, located at specific points along them, which could be obtained graphically from experimental data. This point of departure is adopted in the following algorithm.

Algorithm 1. Whenever axial and transverse, uniaxial experiments are available for a material whose anisotropy is described by a single-fiber family with fiber dispersion being enclosed by a cone, that is, whenever constitutive equations (15) and (17) apply, then measure the following four slopes, and record the necessary stretches and stresses of their tangent points.

i. From a stretch vs. true-stress diagram constructed from a uniaxial experiment whose loading axis was aligned with the fiber direction, measure
   - E_a, which is the slope at $\lambda = 1$;
   - E_f, which is the slope midway through the linear region, and
     - λ_f, the stretch at this tangent point;

- E_h, which is the slope halfway up the heel in the nonlinear region, and
  - λ_h and τ_h, the stretch and stress at this tangent point.

ii. From a stretch vs. true-stress diagram constructed from a uniaxial experiment whose loading axis was normal to the fiber direction, measure

- E_t, which is the slope at $\lambda = 1$.

With these data in hand, estimates for the material constants come from the formulæ

$$\delta = \frac{E_t}{2E_a - E_t}, \quad \mu = E_a \frac{2E_a - E_t}{4E_a - E_t}, \quad \beta = \frac{\lambda_f E_f - E_a}{2}, \quad \tau^\star = \tau_h \frac{\lambda_f E_f - E_a}{\lambda_h E_h - E_a}.$$

We assume here that $\alpha = 0$, as these two experiments lack sensitivity to discriminate α from β.

In this algorithm we chose to plot Cauchy stress τ versus stretch λ. This was a conscious decision, made because it requires minimal messaging of the raw data. Therefore, these data can be easily mapped into another stress/strain pair that may be of interest to someone else, i.e., the data have archival value. Without simultaneous knowledge of the deformation gradient, it is difficult, and often impossible, to convert data from one stress/strain format into another when they are only made available as curves in figures.

Having said this, an alternative method for graphically determining parameters in hypoelastic models undergoing simple extensions, which does manipulate the raw data, would be to plot true stress τ versus the tangent modulus $\lambda \mathrm{d}\tau/\mathrm{d}\lambda$, similar to what's done in [Fung 1967]. However, because methods for numeric differentiation magnify noise in their data streams, and because such data streams tend to be noisy to begin with, it is useful, if not essential, that a smoothing function be used to represent these raw data, from which rates are gotten by differentiating the smoothing function instead of the raw data themselves. The generalized cross-validatory method [Woltring 1986] has been used by the author for this purpose with good effect in other studies, but it was not used here.

4.3. ***Tendon.*** Algorithm 1 applies to experimental data sets where uniaxial extensions have been done on two samples: one where axial extension is in the mean fiber direction, and the other where axial extension is normal to the fiber direction. The experimental data of [Weiss 1994] acquired from human fascia lata belong to this classification.

Figure 3 illustrates how to apply step (i) of Algorithm 1 to the data of [Weiss 1994], where the sample was loaded in the direction of the fibers. Modulus E_a is the tangent to the curve at $\lambda = 1$, which has a measured value of 120 MPa. Modulus E_f is a tangent to the curve at λ_f, which was placed roughly midway along the linear portion of the curve, and has a measured value of 675 MPa at a stretch of 1.06. The critical part in an application of this algorithm is to select the next tangent point. Here we seek a location where the tangent modulus is roughly half that of E_f. Drawing this tangent establishes E_h, which has a measured value of 325 MPa ($\sim 675/2$) at the tangent point $\lambda_h = 1.0112$ and $\tau_h = 2.26$ MPa. This completes step (i) of Algorithm 1.

Step (ii) of Algorithm 1 is much less involved. Here all that is required is to acquire the tangent modulus at $\lambda = 1$ from an experiment where the sample was loaded normal to the fiber direction. Figure 4 presents data from [Weiss 1994]; the tangent modulus E_t has a measured value of 30 MPa. Although the initial tangent moduli only differ by a factor of four between Figures 3 and 4, their local tangent moduli at stretches exceeding 1.03 differ by a factor of well over twenty.

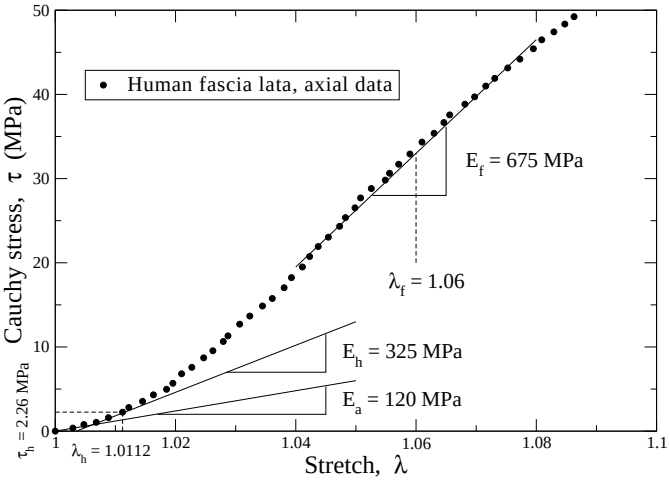

Figure 3. The slopes and their locations pertaining to part (i) of Algorithm 1. The data are from [Weiss 1994, Figure 6.7].

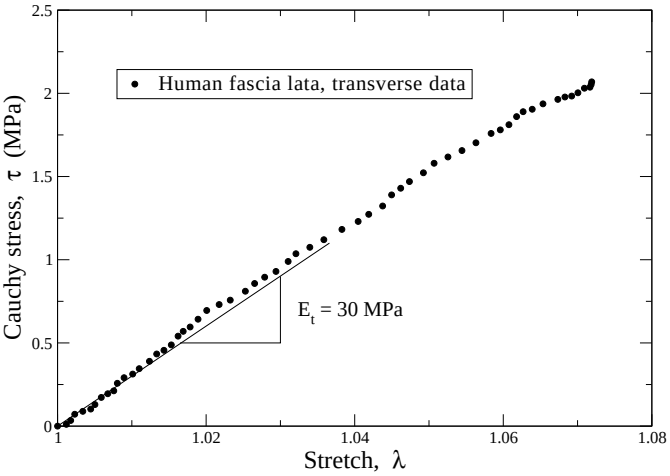

Figure 4. The slope pertaining to part (ii) of Algorithm 1. The data are from in [Weiss 1994, Figure 6.6].

An application of Algorithm 1 to the acquisition of estimates for the model parameters present in (15) and (17) produced the values listed in Table 1, and the dashed response curves displayed in Figures 5 and 6. (Note the different vertical scales.) The parameters listed in this table are the outcome of our first

Parameters	δ	μ/MPa	β/MPa	$\tau^\star$/MPa	R^2
Graphical estimates	0.14±0.07	56±62	300±68	6.5±5.0	0.743
Optimized estimates	0.06±0.018	120±41	225±41	13±5.7	0.996

Table 1. Parameter estimates with 90% confidence intervals for the anisotropic, isochoric, hypoelastic, tissue model (10), obtained by the graphical method of Algorithm 1, and by the numerical method of Appendix B. The parameter α was set to 0 in both cases.

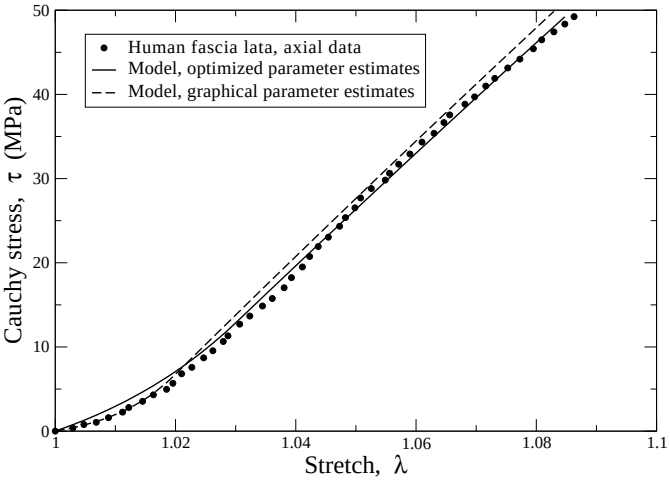

Figure 5. Comparisons between experimental data and values from (15), where the parameters were estimated using the graphical method of Algorithm 1 and the maximum likelihood method of Appendix B. The data are from [Weiss 1994, Figure 6.7].

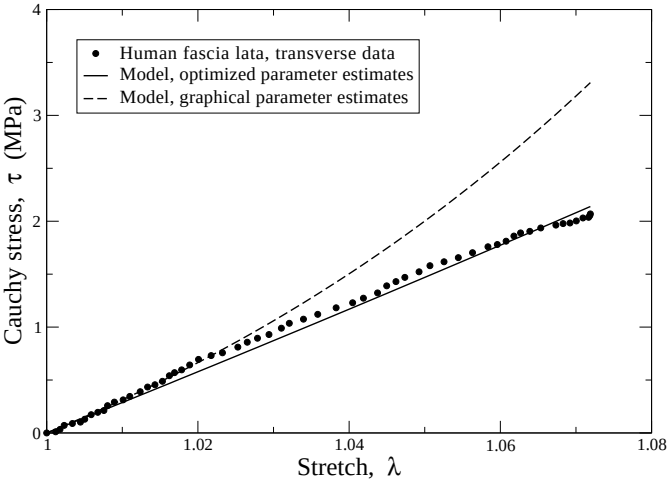

Figure 6. Comparisons between experimental data and (17), where parameters were estimated from the graphical method of Algorithm 1, and the maximum likelihood method of Appendix B. The data are from [Weiss 1994, Figure 6.6].

and only attempt to graphically quantify the tangent moduli utilized by the formulæ in Algorithm 1. The 90% confidence intervals for the graphical estimates were obtained by constructing a covariance matrix for their residuals, as described in Appendix A. Improvements, based on visual inspection, could have likely been obtained by iterating on one's choice of parameters, but that was not done here.

Using these graphical estimates as initial guesses for the parameters, maximum likelihood estimates were then obtained whose values are also listed in Table 1, along with their 90% confidence intervals, and whose responses are plotted as the solid curves in Figures 5 and 6.

5. Discussion

To gain sensitivity between parameters α and β in the hypoelastic tissue models during a parameter estimation will require at least two experiments, each loaded into the nonlinear region of their response, and each with a different hydrostatic state. Experimental data with sufficient sensitivity to discriminate α from β are rare. A document where such a data set will be considered is now being written.

Parameters α and β are confounded in the parameter estimates of this paper, because experiments with the same hydrostatic state have been used for model correlations. We have dealt with this confounding by assigning one or the other of the nonlinear parameters to be zero, based on physical arguments. Consequently, care should be exercised if any of the parameters derived herein are to be used in an actual three-dimensional analysis, as the data sets used to quantify the models, by themselves, are incapable of providing complete sensitivity for all parameters during an optimization.

Isotropic case. The Fung-like parameters α and β are associated with stress/strain responses that grow exponentially in stress with increasing stretch, and because of this, they do not produce responses with tension/compression symmetry. As a general observation, the soft tissues that nature has created to support compressive loads are poor at supporting tensile loads, and vice versa. This is consistent with the influence that parameters α and β have on the overall material response. Hence, one might expect α to be restricted to taking on negative values, and β to be restricted to taking on positive values, as is the case here, but this is only conjecture at this time.

The correlation between theory and experimental data is quite good in Figure 1, with an R^2 statistic of 0.976, and it is exceptional in Figure 2, with an R^2 statistic of 0.999, especially since there are only two adjustable parameters available to the model, due to the fact that the experimental data sets that were fit against belong to just one type of boundary-value problem; namely, simple extension.

Anisotropic case. An advantage of our constitutive equation (10) for describing soft tissues over most models published in the open literature is the relative ease by which it can be applied to tissues with different anisotropic structures. This is because anisotropy is handled through a single, symmetric, material tensor $\bar{\boldsymbol{A}}$ whose independent components establish the relative directional strengths of the anisotropy. Anisotropy tensors for splayed fiber architectures belonging to a single-fiber family with an elliptic projection onto the transverse plane in the reference configuration have been reviewed in [Freed 2008].

The particular relationship between the angle of fiber dispersion $\angle$ and the dispersion parameter δ itself, as it appears in (13), will depend upon the probability distribution function that one selects. Curiously, the mathematical structure of matrix $\bar{\boldsymbol{A}}$ is independent of that choice [Gasser et al. 2006], which is remarkable result. One such possible mapping is given in Table 2.

At first glance, when comparing the two estimated values for the dispersion parameter δ listed in

angle	0°	5°	10°	15°	20°	25°	30°	35°	40°	45°	60°	90°	180°
δ	0	0.02	0.06	0.13	0.23	0.34	0.45	0.54	0.61	0.67	0.78	0.90	1

Table 2. Dispersion parameter δ at various angles of fiber splay for a fiber fan with Gaussian distribution [Freed et al. 2005], where 0° is the limiting case of transverse isotropy and 180° is the other limiting case of planar isotropy.

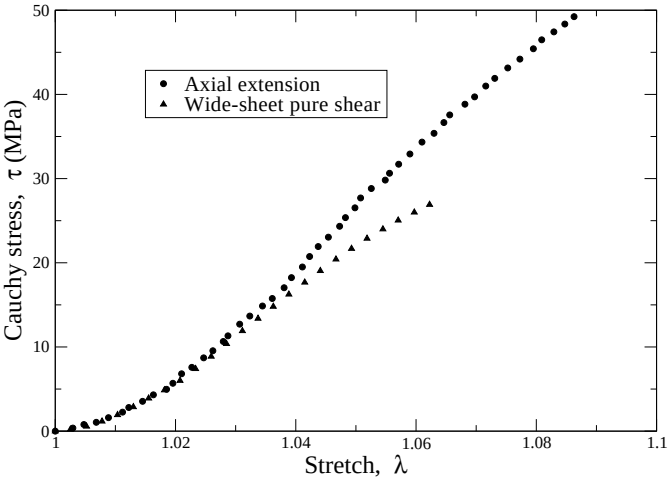

Figure 7. Data for human fascia lata tested in axial extension, and laterally constrained (wide sheet) axial extension, often referred to as pure shear in the rubber literature. The data are from [Weiss 1994, Figures 6.7 and 6.8].

Table 1, obtained from the two different estimation procedures, one might be inclined to think that these estimates are significantly different. However, when viewed through Table 2, we see that these differences correspond to fiber dispersion angles of roughly 10° and 15° (or 5° and 7.5° off the mean) which, from this vantage point, is a rather small difference. Both of these angles seem reasonable for tendon.

Differences between the BCs (19) for laterally-constrained axial extensions and the BCs (15) for simple axial extensions in the strong direction diminish in the neighborhood of transverse isotropy, that is, as $\delta \to 0$. This agrees with the experimental data of Weiss [1994] presented in Figure 7; his experiments were done on human fascia lata. They are plotted together here, and lie one atop the other up to stretches of about 1.03. Beyond this point they begin to diverge because of experimental difficulties, as Weiss states: "The most likely cause of this systematic error is a problem in satisfying the constraint that the lateral stretch was maintained at a value of 1.0." Because these experimental curves are coincident, the laterally-constrained axial experiment brings little added value to the overall process of parameter estimation for tissues whose fiber alignment is fairly strong.

An inspection of Figure 5 for the axial response suggests that the two methods of parameter estimation are equally good. The graphical method does slightly better for stretches below 1.02, while the maximum likelihood method does slightly better for stretches beyond 1.02. Examining the estimates for the shear modulus μ given in Table 1, which controls the response around $\lambda = 1$, one finds a factor of two difference between them. This disparity is exasperated by the relatively short toe region that is present in these data.

An inspection of Figure 6 for the transverse response may lead one to want to draw a different conclusion, but one should not be too hasty. The absolute differences in predicted stresses are less here than they are in Figure 5; the relative differences are, however, significantly greater, which is why the small coefficient of determination reported in Table 1 for the graphical method. Certainly, the correlations are good below a stretch of 1.02 in Figure 6. Above that, the correlation that used estimates from the graphical method starts to pick up an exponential contribution that is not present in the correlation that

used maximum likelihood estimates. The reason for this is the factor of two difference between the values of their dispersion parameters δ. Because their δs differ by a factor of two, the graphical correlation has twice the contribution that the numerical correlation has in the nonlinear region, introduced through the term $2\delta\beta f(\tau)/\lambda$ in (17). This effect is countered in the linear region by a like difference between the estimates for their shear moduli μ.

A close examination of the theoretical curves in the linear response region of Figure 5 finds that they are not exactly linear. There is a small degree of concavity in them with increasing stretch, as there is in the experimental data. This effect is not large, and theory and experiment are consistent in this regard. If fact, theory implies a linear response beyond the toe region only in true stress/strain plots. Also, if one back calculates from the optimized parameters listed in Table 1 to get the fiber modulus E_f, one obtains 650 MPa, which is very close to the graphical value of 675 MPa.

6. Concluding remarks

As a general observation, hypoelasticity seems to be well suited for describing the passive elastic response of soft tissues. The modeling put forward in this paper supports this conclusion, but it is just a first step towards model verification. Many other tissues and boundary-value problems, including FE analyses, need to be modeled with this theory to determine its domain of applicability and its overall usefulness.

Appendix A. Parameter estimation

Here we describe how to obtain maximum likelihood estimates for parameters in models that are described in terms of a system of ODEs, like hypoelasticity. The text [Bard 1974] is somewhat old, but remains an excellent reference for nonlinear parameter estimation techniques. All numerical integrations done in this paper were obtained using the Runge–Kutta integrator introduced in Appendix B.

Assign I to be the number of measured/modeled variables, J to be the number of internal state variables, K to be the number of unknown parameters to be estimated, and N to be the number of experimental observations to be fit against. Let scalar x_n denote the control (or independent) variable at datum point n — for example, stretch — where n ranges from 1 to N. Let the one-dimensional vectors $\boldsymbol{y}_n$ and $\mathfrak{y}(\boldsymbol{\theta}, x_n)$ contain the experimental and theoretical response (or dependent) variables, respectively, at each datum point n, for example, stresses, while $\bar{\boldsymbol{y}} = \frac{1}{N}\sum_{n=1}^{N} \boldsymbol{y}_n$ denotes their experimental mean. And let the K-dimensional vector $\boldsymbol{\theta}$ contain parameters for the model whose values are being sought. This algorithm requires that $N \geq I$ and that $N > K$.

Adopting a standard reduced model for assessing error, let the I-dimensional residual vector $\boldsymbol{r}_n$ at datum point n be defined by

$$\boldsymbol{r}_n(\boldsymbol{\theta}) = \boldsymbol{y}_n - \mathfrak{y}(\boldsymbol{\theta}, x_n) \quad \text{with components} \quad r_{n,i}(\boldsymbol{\theta}) = y_{n,i} - \mathfrak{y}_i(\boldsymbol{\theta}, x_n), \tag{22}$$

in which $r_{n,i}$ denotes the i-th row element of column vector $\boldsymbol{r}_n$, $i = 1, 2, \ldots, I$. Vector $\boldsymbol{r}_n(\boldsymbol{\vartheta})$ is the experimental error at state n whenever $\boldsymbol{\vartheta}$ represents the actual parameters from a model that is 'truth'. The $I \times I$ matrix

$$\boldsymbol{M}(\boldsymbol{\theta}) = \sum_{n=1}^{N} \boldsymbol{r}_n(\boldsymbol{\theta}) \otimes \boldsymbol{r}_n(\boldsymbol{\theta}) \quad \text{with components} \quad M_{ij}(\boldsymbol{\theta}) = \sum_{n=1}^{N} r_{n,i}(\boldsymbol{\theta}) r_{n,j}(\boldsymbol{\theta}) \tag{23}$$

defines the moment of residuals, which will be symmetric positive-definite whenever $\|\boldsymbol{r}_n\| > 0$ for at least I of the N measurements, as each $\boldsymbol{r}_n \otimes \boldsymbol{r}_n$ is at most a rank-1 matrix.

Whenever the residuals $\boldsymbol{r}_n$ from each of the N datum points are independent of one another, and whenever they are normally distributed with the same covariance matrix $\boldsymbol{V}$, then the likelihood $\mathscr{L}$ of $\boldsymbol{\theta}$ being the actual set of parameters $\boldsymbol{\vartheta}$ for a given model $\mathfrak{y}$ is the product of its N probability density functions

$$\begin{aligned}\mathscr{L}[\boldsymbol{r}(\boldsymbol{\theta})|\boldsymbol{V}] = \mathscr{L}(\boldsymbol{\theta}) &= \prod_{n=1}^{N} \frac{1}{\sqrt{(2\pi)^I \det \boldsymbol{V}}} \exp\left(-\tfrac{1}{2}\boldsymbol{r}_n(\boldsymbol{\theta}) \cdot \boldsymbol{V}^{-1}\boldsymbol{r}_n(\boldsymbol{\theta})\right) \\ &= \left(\frac{1}{(2\pi)^I \det \boldsymbol{V}}\right)^{N/2} \exp\left(-\frac{1}{2}\sum_{n=1}^{N} \boldsymbol{r}_n(\boldsymbol{\theta}) \cdot \boldsymbol{V}^{-1}\boldsymbol{r}_n(\boldsymbol{\theta})\right) \\ &= \left(\frac{1}{(2\pi)^I \det \boldsymbol{V}}\right)^{N/2} \exp\left(-\tfrac{1}{2}\operatorname{tr}(\boldsymbol{V}^{-1}\boldsymbol{M}(\boldsymbol{\theta}))\right).\end{aligned} \tag{24}$$

For those cases where the covariance matrix of the residuals $\boldsymbol{V}$ is not known in advance, as is our situation, the natural logarithm of this likelihood function simplifies (24) to [Bard 1974]

$$\ln(\mathscr{L}(\boldsymbol{\theta})) = \frac{N}{2}\left(I\left(\ln\left(\frac{N}{2\pi}\right) - 1\right) - \ln\det \boldsymbol{M}(\boldsymbol{\theta})\right), \tag{25}$$

whose bias-corrected covariance matrix can be determined post-analysis as $\boldsymbol{V} = \frac{I}{IN-K}\boldsymbol{M}(\boldsymbol{\vartheta})$. From this matrix, one can acquire confidence intervals for the parameter estimates, and one can ascertain whether or not the parameters act independent of one another (compare [Bard 1974]).

The Akaike information criterion (AIC) is a powerful tool that blends information theory with statistics for the purpose of objectively selecting the best model from a pool of candidate models [Burnham and Anderson 2002]. A model's log-likelihood, computed by (25), quantifies one of the two terms that make up the AIC statistic; in particular, $\mathrm{AIC} = 2\big(NK/(N-K-1) - \ln \mathscr{L}(\boldsymbol{\vartheta})\big)$, where K varies between models. What AIC brings to the table when modeling soft tissues is discussed in more detail in [Freed and Diethelm 2006].

Maximizing the log-likelihood function of (25) is equivalent to minimizing the objective function

$$\Phi(\boldsymbol{\theta}) = \frac{N}{2}\ln\det \boldsymbol{M}(\boldsymbol{\theta}). \tag{26}$$

The minimization of this objective function can be cast as a linear equation $\boldsymbol{H}\Delta\boldsymbol{\theta} = -\boldsymbol{q}$ that can in turn be solved iteratively via Newton–Raphson iteration[3] so that $\boldsymbol{\theta}_{\nu+1} = \boldsymbol{\theta}_\nu - \boldsymbol{H}_\nu^{-1}\boldsymbol{q}_\nu$, with $\boldsymbol{\theta}_{\nu+1} \to \boldsymbol{\vartheta}$ at convergence. Gauss' approximation for the Hessian $\boldsymbol{H}$ insures that the $K \times K$ matrix $\boldsymbol{H}$ is symmetric positive-definite in that

$$\boldsymbol{H} = \frac{\partial^2\Phi(\boldsymbol{\theta})}{\partial\boldsymbol{\theta}\partial\boldsymbol{\theta}} = 2\sum_{n=1}^{N} \boldsymbol{B}_n^T \boldsymbol{G}\boldsymbol{B}_n \quad \text{with} \quad \boldsymbol{q} = \frac{\partial\Phi(\boldsymbol{\theta})}{\partial\boldsymbol{\theta}} = -2\sum_{n=1}^{N} \boldsymbol{B}_n^T \boldsymbol{G}\boldsymbol{r}_n, \tag{27}$$

[3]Newton–Raphson iteration was actually the genius of Thomas Simpson; see for example [O'Connor and Robertson 2005].

whose embedded metric and gradient matrices, for maximum likelihood estimates, are defined by

$$\boldsymbol{G} = \frac{\partial \Phi(\boldsymbol{M}(\boldsymbol{\theta}))}{\partial \boldsymbol{M}} = \frac{N}{2}\boldsymbol{M}^{-1}(\boldsymbol{\theta}) \quad \text{and} \quad \boldsymbol{B}_n = -\frac{\partial \boldsymbol{r}_n(\boldsymbol{\theta})}{\partial \boldsymbol{\theta}} = \frac{\partial \mathcal{Y}(\boldsymbol{\theta}, \boldsymbol{x}_n)}{\partial \boldsymbol{\theta}}. \tag{28}$$

Different choices for the objective function lead to different constructions for metric $\boldsymbol{G}$; for example, $\boldsymbol{G} = \boldsymbol{I}$ associates with the method of least squares [Bard 1974]. For the optimizations done in this paper, the moment of residuals $\boldsymbol{M}$ was always a fully populated matrix; therefore, least-squares regression is not appropriate here.

Dynamic models. In dynamic models, like hypoelasticity, the I response variables $\mathcal{Y}_i(\boldsymbol{\theta}, \boldsymbol{s}, x)$, $i = 1, 2, \ldots, I$, depend on a set of J internal state variables $s_j(\boldsymbol{\theta}, x)$, $j = 1, 2, \ldots, J$, that are in turn governed by a system of first-order ODEs so that[4]

$$\frac{\mathrm{d}\boldsymbol{s}}{\mathrm{d}x} = \boldsymbol{f}(\boldsymbol{\theta}, \boldsymbol{s}, x) \quad \text{with IC} \quad \boldsymbol{s}(\boldsymbol{\theta}, x_0) = \boldsymbol{s}_0, \tag{29}$$

implying that there are now $N + 1$ experimental datum points, with the model being calibrated at the initial state $\mathcal{Y}(\boldsymbol{\theta}, \boldsymbol{s}_0, x_0) = \boldsymbol{y}_0$. It therefore follows from the chain rule that gradient $\boldsymbol{B}_n$ now becomes

$$\boldsymbol{B}_n = \frac{\partial \mathcal{Y}(\boldsymbol{\theta}, \boldsymbol{s}_n, x_n)}{\partial \boldsymbol{\theta}} + \frac{\partial \mathcal{Y}(\boldsymbol{\theta}, \boldsymbol{s}_n, x_n)}{\partial \boldsymbol{s}_n}\frac{\partial \boldsymbol{s}_n}{\partial \boldsymbol{\theta}}, \tag{30}$$

whose unknown matrix of coefficients $\partial \boldsymbol{s}_n / \partial \boldsymbol{\theta}$ is a solution to an ODE called the sensitivity equation

$$\frac{\mathrm{d}}{\mathrm{d}x}\frac{\partial \boldsymbol{s}}{\partial \boldsymbol{\theta}} = \frac{\partial \boldsymbol{f}}{\partial \boldsymbol{\theta}} + \frac{\partial \boldsymbol{f}}{\partial \boldsymbol{s}}\frac{\partial \boldsymbol{s}}{\partial \boldsymbol{\theta}} \quad \text{with IC} \quad \frac{\partial \boldsymbol{s}(\boldsymbol{\theta}, x_0)}{\partial \boldsymbol{\theta}} = \frac{\partial \boldsymbol{s}_0}{\partial \boldsymbol{\theta}}, \tag{31}$$

that needs to be integrated simultaneously with (29), as they constitute a coupled system. The writing of (31) requires $\boldsymbol{s}$ to be continuous and sufficiently differentiable in x and $\boldsymbol{\theta}$ so that the left-hand side $\frac{\partial}{\partial \boldsymbol{\theta}}\frac{\mathrm{d}\boldsymbol{s}}{\mathrm{d}x}$ can be reordered to read as $\frac{\mathrm{d}}{\mathrm{d}x}\frac{\partial \boldsymbol{s}}{\partial \boldsymbol{\theta}}$.

Dynamic models also differ from static ones in that the sums to N in (27) for the Hessian $\boldsymbol{H}$ and gradient $\boldsymbol{q}$ now start at 0, instead of 1, so that the initial conditions can be accounted for. This is essential whenever initial conditions are to be amongst the parameters being estimated in an optimization.

Coefficient of determination. The R^2 statistic is not uniquely defined for nonlinear optimizations, and many schemes have been proposed in the literature. The R^2 statistic chosen for use here was derived in [Buse 1973] for the method of generalized least squares, and is selected because of its relative ease in application, once log-likelihood estimates $\hat{\boldsymbol{\theta}}$ are in hand, and because of its applicability to the maximum likelihood method. It is defined by

$$R^2 = 1 - \sum_{n=1}^{N} \frac{\boldsymbol{r}_n(\boldsymbol{\theta}) \cdot \boldsymbol{M}(\boldsymbol{\theta})^{-1}\boldsymbol{r}_n(\boldsymbol{\theta})}{\sum_{\nu=1}^{N}(\boldsymbol{y}_\nu - \bar{\boldsymbol{y}}) \cdot \boldsymbol{M}(\boldsymbol{\theta})^{-1}(\boldsymbol{y}_\nu - \bar{\boldsymbol{y}})}\bigg|_{\boldsymbol{\theta}=\hat{\boldsymbol{\theta}}}, \tag{32}$$

[4]In some models, like those in (3) and (10), there is no difference between the response and internal state variables. In other models, there is a difference; for example, in the fiber-matrix theory presented in [Freed 2008], the fiber and matrix stresses $\boldsymbol{T}^f$ and $\boldsymbol{T}^m$ are internal state variables that relate to the response variable, stress $\boldsymbol{T}$, via an equation of state known as the rule of mixtures.

where the covariance matrix for the residuals $\boldsymbol{V}$ has been replaced by the moment of residuals $\boldsymbol{M}$, because they become proportional whenever $\boldsymbol{M}(\boldsymbol{\theta})$ is evaluated with the maximum likelihood estimates $\boldsymbol{\vartheta}$.

Appendix B. A new 4(3) Runge–Kutta integrator

Integrations done in this paper were achieved using the explicit 4(3) Runge–Kutta integrator whose coefficients are given in Table 3. This fourth-order Runge–Kutta method in five stages with an embedded third-order method solves the nonlinear ODE $\mathrm{d}\boldsymbol{y}/\mathrm{d}x = \boldsymbol{f}(x, \boldsymbol{y})$ with IC $\boldsymbol{y}(x_0) = \boldsymbol{y}_0$ via the formulæ

$$\begin{aligned}
\boldsymbol{k}_1 &= \boldsymbol{f}(x_i, \boldsymbol{y}_i),\\
\boldsymbol{k}_2 &= \boldsymbol{f}(x_i + c_2 h, \boldsymbol{y}_i + h a_{21}\boldsymbol{k}_1),\\
\boldsymbol{k}_3 &= \boldsymbol{f}(x_i + c_3 h, \boldsymbol{y}_i + h(a_{31}\boldsymbol{k}_1 + a_{32}\boldsymbol{k}_2)),\\
\boldsymbol{k}_4 &= \boldsymbol{f}(x_i + c_4 h, \boldsymbol{y}_i + h(a_{41}\boldsymbol{k}_1 + a_{42}\boldsymbol{k}_2 + a_{43}\boldsymbol{k}_3)),\\
\boldsymbol{k}_5 &= \boldsymbol{f}(x_i + c_5 h, \boldsymbol{y}_i + h(a_{51}\boldsymbol{k}_1 + a_{52}\boldsymbol{k}_2 + a_{53}\boldsymbol{k}_3 + a_{54}\boldsymbol{k}_4)),\\
\boldsymbol{y}_{i+1} &= \boldsymbol{y}_i + h(b_1\boldsymbol{k}_1 + b_2\boldsymbol{k}_2 + b_3\boldsymbol{k}_3 + b_4\boldsymbol{k}_4 + b_5\boldsymbol{k}_5),\\
\hat{\boldsymbol{y}}_{i+1} &= \boldsymbol{y}_i + h(\hat{b}_1\boldsymbol{k}_1 + \hat{b}_2\boldsymbol{k}_2 + \hat{b}_3\boldsymbol{k}_3 + \hat{b}_4\boldsymbol{k}_4 + \hat{b}_5\boldsymbol{k}_5),
\end{aligned} \tag{33}$$

where $h = x_{i+1} - x_i$ is the step size. We derived the coupling coefficients (the a_{ij} in the center tableau of Table 3) for this integrator from the four order conditions for a third-order Runge–Kutta method, and from the eight order conditions for a fourth-order method [Hairer et al. 1993]. This integrator combines the quadrature points (the c_i) and weights (the b_j) from Kutta's three-eights rule [1901], which is fourth-order accurate, with those from Simpson's rule[5] (establishing c_3 and the $\hat{b}_j$), which is third-order accurate. These quadrature/weight schemes arise from Lagrange interpolation, and are manifest in FE theory whenever discrete nodal forces are used to represent uniform, external, pressure loadings that in turn produce uniform states of stress within an element [Cook et al. 2002]. It is this continuity of a

0					
c_2	a_{21}				
c_3	a_{31}	a_{32}			
c_4	a_{41}	a_{42}	a_{43}		
c_5	a_{51}	a_{52}	a_{53}	a_{54}	
$\boldsymbol{y}$	b_1	b_2	b_3	b_4	b_5
$\hat{\boldsymbol{y}}$	$\hat{b}_1$	$\hat{b}_2$	$\hat{b}_3$	$\hat{b}_4$	$\hat{b}_5$

0					
1/3	1/3				
1/2	0	1/2			
2/3	$-x/3$	x	$2(1-x)/3$		
1	x	$2-3x$	$2(x-1)$	1	
$\boldsymbol{y}$	1/8	3/8	0	3/8	1/8
$\hat{\boldsymbol{y}}$	1/6	0	2/3	0	1/6

0					
1/3	1/3				
1/2	0	1/2			
2/3	–2/9	2/3	2/9		
1	2/3	0	–2/3	1	
$\boldsymbol{y}$	1/8	3/8	0	3/8	1/8
$\hat{\boldsymbol{y}}$	1/6	0	2/3	0	1/6

Table 3. The Butcher tableau for a generic, five-stage, Runge–Kutta method is given on the left. The Butcher tableau for a new, embedded, 4(3) Runge–Kutta method in 5 stages is presented in the middle, where x has been set to 2/3 in the right tableau, which is near optimum.

[5] "Simpson's rule had been used by Johannes Kepler in the construction of an approximate method for computing the volume of wine casks. This work of Kepler's was published in 1615, almost 100 years before Simpson was born, in his treatise with the title *Nova stereometria doliorum vinariorum* (A new stereometry [i.e. method for the computation of the volume] for wine casks). Hence, at least in the German speaking literature, Simpson's rule is sometimes called 'Kepler's cask rule'." (Private communication, Prof. Kai Diethelm, Technische Universität Braunschweig.)

uniform input producing a uniform output through a discretized interface that motivated the development of this integrator.

With the quadrature points and weights established a priori, the resulting twelve order conditions, several being satisfied trivially by the preassigned quadrature points and weights, require that the unknown elements in the bottom two rows of the coupling matrix be described in terms of a single parameter, as shown in the middle tableau. The selected value for this parameter, $x = 2/3$, yields the simple set of coupling coefficients listed in the rightmost tableau of Table 3, which roughly minimize the error coefficients of this integrator. These error coefficients are measures of how far the order conditions are from being satisfied for the next higher-order set. For this integrator, they are ($-1/54$, $1/36$, $-1/9$, $119/144$, $-1/9$, $-23/27$, $-1/9$, $1/36$, $2/9$) for solution $\boldsymbol{y}$, and (0, 0, $1/9$, $1/9$) for solution $\hat{\boldsymbol{y}}$.

The PI (proportional integral) controller of [Gustafsson et al. 1988] was used to dynamically adjust the step size of integration. This controller is driven by a local error estimate $\boldsymbol{y} - \hat{\boldsymbol{y}}$ that, for the integrator in Table 3, has contributions arising from each of the five quadrature locations, which is another desirable feature of our integrator.

Acknowledgement

The author thanks Profs. Margo Lillie and Janice Miller-Young for graciously providing him with raw data from their laboratories that they and their colleagues had published in the journal literature. The data from Prof. Jeffery Weiss' PhD thesis [Weiss 1994] were redigitized using the software package g3data (http://www.frantz.fi/software/g3data.php).

References

[Aaron and Gosline 1981] B. B. Aaron and J. M. Gosline, "Elastin as a random-network elastomer: a mechanical and optical analysis of single elastin fibers", *Biopolymers* **20**:6 (1981), 1247–1260.

[Bard 1974] Y. Bard, *Nonlinear parameter estimation*, Academic Press, New York, 1974.

[Burnham and Anderson 2002] K. P. Burnham and D. R. Anderson, *Model selection and multimodel inference: a practical information-theoretic approach*, 2nd ed., Springer, New York, 2002.

[Buse 1973] A. Buse, "Goodness of fit in generalized least squares estimation", *Am. Stat.* **27**:3 (1973), 106–108.

[Cook et al. 2002] R. D. Cook, D. S. Malkus, M. E. Plesha, and R. J. Witt, *Concepts and applications of finite element analysis*, 4th ed., Wiley, New York, 2002.

[Criscione et al. 2003] J. C. Criscione, M. S. Sacks, and W. C. Hunter, "Experimentally tractable, pseudo-elastic constitutive law for biomembranes, II: Application", *J. Biomech. Eng.* (*ASME*) **125**:1 (2003), 100–105.

[Dienes 1979] J. K. Dienes, "On the analysis of rotation and stress rate in deforming bodies", *Acta Mech.* **32**:4 (1979), 217–232.

[Dienes 1987] J. K. Dienes, "Theory of deformation, 1: Kinematics", Technical Report LA–11063–MS, Vol. 1, Los Alamos National Laboratory, December 1987.

[Freed 2008] A. D. Freed, "Anisotropy in hypoelastic soft-tissue mechanics, I: Theory", *J. Mech. Mater. Struct.* **3**:5 (2008), 911–928.

[Freed and Diethelm 2006] A. D. Freed and K. Diethelm, "Fractional calculus in biomechanics: a 3D viscoelastic model using regularized fractional derivative kernels with application to the human calcaneal fat pad", *Biomech. Model. Mechanobiol.* **5**:4 (2006), 203–215.

[Freed and Doehring 2005] A. D. Freed and T. C. Doehring, "Elastic model for crimped collagen fibrils", *J. Biomech. Eng.* (*ASME*) **127**:4 (2005), 587–593.

[Freed et al. 2005] A. D. Freed, D. R. Einstein, and I. Vesely, "Invariant formulation for dispersed transverse isotropy in aortic heart valves: an efficient means for modeling fiber splay", *Biomech. Model. Mechanobiol.* **4**:2–3 (2005), 100–117.

[Fung 1967] Y. C. Fung, "Elasticity of soft tissues in simple elongation", *Am. J. Physiol.* **213**:6 (1967), 1532–1544.

[Gasser et al. 2006] T. C. Gasser, R. W. Ogden, and G. A. Holzapfel, "Hyperelastic modelling of arterial layers with distributed collagen fibre orientations", *J. R. Soc. Interface* **3**:6 (2006), 15–35.

[Green and Naghdi 1965] A. E. Green and P. M. Naghdi, "A general theory of an elastic-plastic continuum", *Arch. Ration. Mech. An.* **18**:4 (1965), 251–281.

[Gustafsson et al. 1988] K. Gustafsson, M. Lundh, and G. Söderlind, "A PI stepsize control for the numerical solution of ordinary differential equations", *BIT* **28**:2 (1988), 270–287.

[Hairer et al. 1993] E. Hairer, S. P. Nørsett, and G. Wanner, *Solving ordinary differential equations, I: Nonstiff problems*, 2nd ed., Springer Series in Computational Mathematics **8**, Springer, Berlin, 1993.

[Holzapfel 2000] G. A. Holzapfel, *Nonlinear solid mechanics: a continuum approach for engineering*, Wiley, Chichester, 2000.

[Holzapfel et al. 2002] G. A. Holzapfel, T. C. Gasser, and M. Stadler, "A structural model for the viscoelastic behavior of arterial walls: continuum formulation and finite element analysis", *Eur. J. Mech. A Solids* **21**:3 (2002), 441–463.

[Kutta 1901] W. Kutta, "Beitrag zur näherungsweisen Integration totaler Differentialgleichungen", *Z. Math. Phys.* **46** (1901), 435–453.

[Miller-Young et al. 2002] J. E. Miller-Young, N. A. Duncan, and G. Baroud, "Material properties of the human calcaneal fat pad in compression: experiment and theory", *J. Biomech.* **35**:12 (2002), 1523–1531.

[Niederer et al. 2004] P. F. Niederer, P. P. Lunkenheimer, and C. W. Cryer, "On the significance of fiber branching in the human myocardium", *Biomech. Model. Mechanobiol.* **3**:1 (2004), 1–5.

[O'Connor and Robertson 2005] J. J. O'Connor and E. F. Robertson, "Thomas Simpson", online biography in the *MacTutor History of Mathematics*, 2005, Available at http://www-history.mcs.st-and.ac.uk/Biographies/Simpson.html.

[Ogden 1984] R. W. Ogden, *Non-linear elastic deformations*, Wiley, New York, 1984. Republished by Dover, Mineola, NY, 1997.

[Oldroyd 1950] J. G. Oldroyd, "On the formulation of rheological equations of state", *Proc. R. Soc. Lond. A* **200**:1063 (1950), 523–541.

[Rivlin and Smith 1969] R. S. Rivlin and G. F. Smith, "Orthogonal integrity basis for N symmetric matrices", pp. 121–141 in *Contributions to mechanics*, edited by D. Abir, Pergamon, New York, 1969.

[Treloar 1975] L. R. G. Treloar, *The physics of rubber elasticity*, 3rd ed., Clarendon, Oxford, 1975.

[Truesdell 1955] C. Truesdell, "Hypo-elasticity", *Indiana Univ. Math. J.* **4**:1 (1955), 83–133.

[Weiss 1994] J. A. Weiss, *A constitutive model and finite element representation for transversely isotropic soft tissues*, Ph.D. thesis, University of Utah, December 1994.

[Woltring 1986] H. J. Woltring, "A Fortran package for generalized, cross-validatory spline smoothing and differentiation", *Adv. Eng. Software* **8**:2 (1986), 104–113.

Received 3 Sep 2008. Revised 4 Jun 2009. Accepted 4 Jun 2009.

ALAN D. FREED: adfreed@svsu.edu
Saginaw Valley State University, 202 Pioneer Hall, 7400 Bay Road, University Center, MI 48710, United States